Plant Stress 21 (2026) 101438

Contents lists available at ScienceDirect

Plant Stress

journal homepage: www.sciencedirect.com/journal/plant-stress

Pst DC3000 volatiles reprogram Arabidopsis root architecture through ion/redox signaling, plasmodesmal gating and PIN auxin transporters

Chidananda Nagamangala Kanchiswamy [a,1], Ivan A. Paponov [b,1], Mickael Malnoy [c], Francesco Caldo [a], Suruchi Roychoudhry [d], Massimo E. Maffei [a,*]

[a] Plant Physiology Unit, Department of Life Sciences and Systems Biology, University of Turin, Turin 10135, Italy
[b] Department of Food Science, Aarhus University, Aarhus 8000, Denmark
[c] Research and Innovation Centre, Edmund Mach Foundation, San Michele all'Adige 38098, Italy
[d] Centre for Plant Sciences, University of Leeds, Leeds LS2 9JT United Kingdom

ARTICLE INFO

Keywords:
Microbial volatiles
Root system architecture
Symplastic gating
FLS2
Auxin transport

ABSTRACT

Microbial volatile organic compounds (mVOCs) provide early chemical cues of microbial activity in the rhizosphere, yet how plants translate these signals into coordinated intracellular responses and developmental outcomes remains poorly understood. Here we show that mVOCs from *Pseudomonas syringae* pv. *tomato* DC3000 (*Pst* DC3000) remodel *Arabidopsis thaliana* root system architecture (RSA) by inhibiting primary root elongation, reducing lateral root formation, and altering the lateral root gravitropic setpoint angle. Live-cell imaging revealed that *Pst* DC3000 mVOCs trigger rapid Ca^{2+} and K^+ fluxes accompanied by reactive oxygen species (ROS) and nitric oxide (NO) accumulation, followed by callose deposition at plasmodesmata. Genetic and pharmacological dissection uncoupled distinct signaling modules: *fls2* mutants lost the early H_2O_2 burst and showed delayed NO production yet retained wild-type levels of plasmodesmatal callose. This demonstrates that FLS2 functions as a genetic coordinator of early redox timing rather than a mediator of symplastic gating. In contrast, the *pdko3* mutant (pdlp1/2/3) suppressed Ca^{2+}, ROS and early NO responses, indicating that plasmodesmal components are essential for early signal propagation. Pharmacological inhibition of K^+ channels eliminated callose deposition in Col-0 roots, placing K^+ influx upstream of PDLP–PMR4-dependent plasmodesmal regulation. At the developmental level, *Pst* DC3000 mVOCs induced expression of *PDLP2, PDLP3* and *PDLP4* and reconfigured auxin signaling and PIN auxin transporter expression, including AXR1-dependent DR5 activation, transient PIN1 induction and sustained PIN3 repression, ultimately driving root architectural remodeling. Finally, the bacterial volatile 2-methylbutanoic acid partially recapitulated these effects, indicating that full RSA reprogramming depends on the combined action of multiple mVOCs.

Introduction

Plants continuously monitor the rhizosphere for microbial threats and beneficial interactions, adjusting their development and immunity accordingly (Wankhade et al., 2025). Among the chemical cues that shape these decisions, microbial volatile organic compounds (mVOCs) have emerged as key mediators of plant–microbe communication (Kanchiswamy et al., 2015; Parmagnani et al., 2023). Unlike water-borne, non-volatile elicitors, mVOCs diffuse through air-filled soil pores and can influence distant tissues, providing long-range, anticipatory cues before physical pathogen contact (Garbeva and Weisskopf, 2020; Chen and Liu, 2024).

Root system architecture (RSA) is highly plastic and is continuously remodeled in response to environmental cues and biotic interactions (Gifford et al., 2024). RSA traits, including primary root elongation, lateral root formation, and the lateral root gravitropic setpoint angle, are regulated by hormone networks, with auxin signaling and polar auxin transport acting as central executors of developmental patterning (Dastidar et al., 2012; Osmont et al., 2007). While RSA plasticity is a well-documented response to biotic stress, the molecular mechanisms that convert an airborne chemical signal into a structural developmental output remain poorly understood. Bacterial volatile blends, including

* Corresponding author.
E-mail address: massimo.maffei@unito.it (M.E. Maffei).
[1] these authors contributed equally

https://doi.org/10.1016/j.stress.2026.101438
Received 25 February 2026; Received in revised form 11 May 2026; Accepted 31 May 2026
Available online 1 June 2026

those emitted by phytopathogens, can modulate plant growth and activate defense programs (Ryu et al., 2004; Ryu et al., 2003; Sharifi and Ryu, 2018; Parmagnani et al., 2023). However, for *Pseudomonas syringae* pv. *tomato* DC3000 (*Pst* DC3000), a foliar pathogen that can also colonise Arabidopsis roots (Lakshmanan et al., 2012), the mechanisms by which volatile-triggered signaling is routed into defined developmental outputs and which signaling modules connect early perception to root architectural remodeling remain largely uncharacterized.

Three open questions motivate the present study. (i) Do bacterial volatiles engage canonical pattern-recognition receptor (PRR) modules? FLS2, the LRR receptor kinase that perceives the flagellin epitope flg22 (Zipfel et al., 2004), is specialised for proteinaceous ligands and would not be expected to bind low-molecular-weight volatile compounds. Whether mVOCs nevertheless feed into the FLS2 signaling architecture — for example by integrating stress-derived reactive oxygen species (ROS) or by altering FLS2 abundance — has not been tested, and constitutes a non-canonical extension of PRR function that this study is designed to examine. (ii) How do early ion (Ca^{2+}, K^{+}) and redox (ROS, nitric oxide; NO) responses interface with plasmodesmata-located proteins (PDLPs) and the callose synthase PMR4 to produce symplastic gating (Lim et al., 2016; Lee et al., 2011a; Wang et al., 2013; Lee et al., 2011b)? (iii) Are these early events causally linked to longer-term reprogramming of the auxin transport machinery (Semeradova et al., 2020) that ultimately remodels RSA?

Resolving these questions requires a system in which volatile cues can be delivered without confounding direct contact between bacteria and plant tissues. To this end we used a headspace co-cultivation (HSCC) system in which *A. thaliana* seedlings (upper compartment, half-strength MS medium) and *Pst* DC3000 cultures (lower compartment, NA II medium) are physically separated, so that the only molecules exchanged between them are airborne (Parmagnani et al., 2023).

Calcium and potassium fluxes, together with ROS and nitric oxide NO serve as key second messengers in plant stress signaling (Zhao et al., 2025; Kolupaev et al., 2015), yet their specific roles in volatile-triggered signaling and their integration with PD- and auxin-dependent modules have not been systematically examined. Moreover, while individual volatiles have often been studied in isolation (Fincheira and Quiroz, 2018; Garbeva and Weisskopf, 2020; Kanchiswamy et al., 2015), it remains unclear to what extent single compounds recapitulate the effects of complete bacterial volatile blends and whether mixture effects (additive or non-additive) contribute to biological activity.

We therefore hypothesized that *Pst* DC3000 mVOCs elicit early ion and redox signaling that engages immune- and plasmodesmata-associated modules and intersects with auxin signaling to reprogram RSA. To test this, we used time-resolved ion and redox reporters together with genetic perturbation of immune- and plasmodesmata-associated components (*fls2, pmr4, pdko3*) and targeted pharmacology (TEA^{+}) to determine how early signaling dynamics connect to plasmodesmatal callose deposition and how these responses are integrated with auxin signaling and PIN regulation to shape RSA. Finally, we assessed the contribution of 2-methylbutanoic acid as a major volatile component of the *Pst* DC3000 blend.

Material and methods

Plant materials and genetic lines

Experiments were conducted using *Arabidopsis thaliana* (L.) ecotype Columbia-0 (Col-0) as the wild-type background. The following mutant lines were used: the flagellin receptor mutant *fls2*, the callose synthase mutant *pmr4-1*, and the triple mutant *pdko3* (*pdlp1 pdlp2 pdlp3*). All mutants were in the Col-0 background. The *fls2* and *pmr4* mutants were obtained from The Arabidopsis Information Resource (TAIR) (https://www.arabidopsis.org), whereas *pdko3* and PDLP::GUS mutants were kindly provided by Dr Christine Faulkner (John Innes Centre, Norwich, UK).

For signaling and transport assays, the following reporter lines were utilized: *PIN1::GUS, PIN3::GUS, PIN1::GFP* and *PIN3::GFP* lines, as well as *FLS2::FLS2-GFP*, which were obtained from the TAIR. To investigate auxin signaling and its dependence on the AXR1 pathway, we utilized the synthetic auxin-responsive reporter DR5::GUS in the wild-type Col-0 background, as well as the mutant background line *axr1-12 DR5::GUS*, in which DR5::GUS was introgressed into the loss-of-function axr1-12 mutant background. Quantitative PCR (qPCR) analysis for *AXR1* and *PIN* genes was performed using wild-type Col-0 seedlings. The *PDLP2::GUS, PDLP3::GUS, PDLP4::GUS* and *PDLP5::GUS* reporter lines were kindly provided by Dr Christine Faulkner (John Innes Centre, Norwich, UK).

Surface sterilization of *A. thaliana* Col-0 seeds was performed using ethanol (70%) for 2 min and 5% $Ca(ClO)_2$ for 5 min, followed by four rinses with autoclaved water. Sterilized seeds were then cultivated on headspace co-cultivation systems, containing in the upper part half-strength Murashige–Skoog medium (MS medium, Sigma, Milan, Italy) and in the lower part a nutrient agar II (NA II; peptone from casein 3.5 gL^{-1}, peptone from meat 2.5 gL^{-1}, peptone from gelatin 2.5 gL^{-1}, yeast extract 1.5 gL^{-1}, NaCl 5 gL^{-1}, agar–agar 15 gL^{-1}, pH 7.2), as previously described (Parmagnani et al., 2023). Following a 3-day vernalization at 4 °C in the complete darkness, a growth chamber was used to grow the seeds with a 16 h light/8 h dark cycle with approximately 70 μmol photons m^{-2} s^{-1} fluorescent light, at 22 °C and 60% relative humidity.

Bacterial strain

The bacterial pathogen *Pseudomonas syringae* pv. *tomato* (*Pst*) strain DC3000, acquired from Dr. Malnoy's Lab bacterial collection, was used as the source of mVOCs. Cultures were grown on King's B (KB) medium supplemented with rifampicin (50 μg/mL) at 28 °C for 24 h. For co-cultivation experiments, bacterial cells were harvested, washed twice with sterile 10 mM $MgCl_2$, and adjusted to an optical density (OD_{600}) of 0.2 (corresponding to approximately 1×10^8 CFU/mL). To ensure uniformity, each experimental partition was inoculated with 20 μL of this suspension (totaling about 2×10^6 CFU per Petri plate).

Headspace co-cultivation (HSCC) procedure

Co-cultivation was performed using a modified HSCC system as previously described (Parmagnani et al., 2023). Briefly, *A. thaliana* seedlings were grown on one side of a partitioned squared (12 × 12 × 1 cm) Petri plate containing half-strength MS medium. At 5 days post-germination, the opposite partition was inoculated with 20 μL of the *Pst* DC3000 suspension at different time intervals (from 30 min to 24 h). Control plates received 20 μL of sterile 10 mM $MgCl_2$. Plates were sealed with a double layer of Parafilm to allow for the accumulation of mVOCs while preventing physical contact between the bacteria and the plants. For subsequent molecular analysis, roots and shoots of *A. thaliana* seedlings were rapidly frozen in liquid N_2 and maintained at −80 °C.

Identification of 2-methylbutanoic acid by SBSE/GC–MS

Volatile compounds emitted by *Pst* DC3000 were collected by stir bar sorptive extraction (SBSE) using a Twister stir bar (Gerstel GmbH & Co. KG, Mülheim an der Ruhr, Germany) attached to the inner surface of the Petri dish cover by an external magnet. After 16 h of headspace exposure, the stir bar was placed into a Gerstel Thermal Desorption Unit (TDU) coupled to a Cooled Injection System (CIS) and analysed by GC–MS following Parmagnani et al. (2023). TDU programme: 36 °C (0.5 min) → 25 °C min^{-1} → 260 °C (5 min); splitless mode; He at 50 mL min^{-1}. CIS programme: 50 °C (0.2 min) → 12 °C s^{-1} → 290 °C (3 min); splitless for the first 6 min, then split 1:20. Chromatographic separation was performed on an HP-5 capillary column (5% diphenyl, 95% dimethylsiloxane; HP 19091J-433); oven programme 50 °C → 3 °C min^{-1} → 200 °C (10 min) → 10 °C min^{-1} → 290 °C (10 min); He carrier at 1.0 mL

min^{-1}. Detection used a quadrupole in EI mode at 70 eV (autotune); MS source 150 °C, quadrupole 230 °C. Compound identification combined: (i) mass-spectrum comparison with the NIST 14 library; (ii) calculation of Kovàts retention indices for comparison with literature and in-house databases; and (iii) direct comparison with the authentic 2-methylbutanoic acid reference standard (Sigma-Aldrich, ≥ 98% purity, Cat. No. 193070). Sterile LB medium served as the bacterium-free headspace control. The resulting identification parameters and verification results for 2-MBA are summarised in Supplementary Table S1.

Synthetic 2-methylbutanoic acid bioassays

To assess the biological activity of the previously identified volatile 2-methylbutanoic acid (2-MBA) (see Supplementary Table S1), synthetic 2-MBA (Sigma-Aldrich) was dissolved in dimethyl sulfoxide (DMSO). In the HSCC system, 2-MBA was applied to the lower compartment at a final concentration representative of the bacterial headspace. Control seedlings were exposed to an equivalent volume of pure DMSO to account for any carrier effects. Seedlings were cultivated for 14 days post-exposure, after which primary root length, lateral root number, lateral root gravitropic setpoint angle (LRGSA) and total leaf area were quantified as described for the full volatile blend (n = 75 seedlings per treatment).

Root architecture and leaf parameters

Root architecture parameters and leaf area were quantified for Col-0, *fls2, pmr4-1,* and *pdko3* seedlings. At 14 days after the initial treatment, the following parameters were measured: leaf area, root length, the number of lateral roots per plant, and the lateral root gravitropic setpoint angle (LRGSA). These measurements were performed using ImageJ (http://imagej.nih.gov/ij) following established protocols (Roychoudhry et al., 2023).

Confocal laser scanning fluorescence analysis of intracellular calcium variations, voltage- and ligand-gated K^+ channels activity, H_2O_2 and NO production

A Nikon Eclipse C1 spectral confocal laser scanning microscope was employed for all fluorescence analyses, and the resulting digital images were processed using NIH image software, as previously detailed (Mithöfer et al., 2009). The exposure time of *A. thaliana* to *Pst* DC3000 mVOCs for these analyses varied from 30 min to 24 h to capture the specific kinetics of each cellular response (e.g., rapid calcium influx versus a more gradual accumulation of H_2O_2 and NO). Intracellular calcium fluctuations were monitored using calcium orange (stock in DMSO, Molecular Probes, Leiden, Netherlands). *A. thaliana* roots and shoots exposed to *Pst* DC3000 mVOC for durations ranging from 30 min to 3 h were incubated with 5 μM calcium orange for 30 min in the dark and then observed with a Krypton/Argon laser at 488 nm, with emission detected using a 500–540 nm band-pass filter and a 650 nm long-pass filter. Control samples consisted of unexposed tissues treated with 5 μM calcium orange solution. Voltage- and ligand-gated K^+ channels were investigated at time points from 30 min to 3 h using the FluxOR™ potassium ion channel assay kit, supplied by Invitrogen (Molecular Probes, Leiden, The Netherlands). Following the manufacturer's recommendations, *A. thaliana* seedlings, either treated with *Pst* DC3000 mVOCs or left untreated, were incubated in darkness for 60 min with 100 μl of loading buffer (a mixture of deionized water, FluxOR™ assay buffer, and probenecid). Immediately preceding microscopic observation, 50 μl of stimulus buffer (comprising deionized water, FluxOR™ chloride-free buffer, K_2SO_4, and Tl_2SO_4), prepared as per the manufacturer's specifications, was added. Subsequently, fluorescence emission was quantified using previously established methods (Bricchi et al., 2013). Steady-state hydrogen peroxide (H_2O_2) production in *A. thaliana* roots and shoots exposed to *Pst* DC3000 mVOC was assessed using 50 μM 10-Acetyl-3,7-dihydroxyphenoxazine (Amplex Red, Molecular Probes, Leiden, The Netherlands). Fluorescence measurements were taken after 60 min incubation in the dark from 30 min to 24 h, as previously described (Maffei et al., 2006). Scans were recorded using an Argon laser (458 nm/5 mW; 476 nm/5 mW; 488 nm/20 mW; 514 nm/20 mW) and HeNe lasers (543 nm/1.20 mW and 633 nm/10 mW). Nitric oxide (NO) detection was achieved using 4,5-diaminofluorescein diacetate (DAF-FM DA, Molecular Probes, Leiden, The Netherlands) in *A. thaliana* roots and shoots exposed for 30 min to 24 h. NO detection was performed by applying 50 μL of a loading solution containing 10 μM DAF-FM DA. After a 60 min period of incubation, the resulting fluorescence was then stimulated using an argon laser at an excitation wavelength of 488 nm, and the emitted light was captured through a band-pass filter with a range of 508 to 525 nm. To elucidate the specific role of NO, tissues were treated with carboxy-2-phenyl-4,4,5,5-tetra-methylimidazolinone-3-oxide-1-oxyl (cPTIO, Sigma, Milan, Italy), a known NO scavenger dissolved in DMSO at a final concentration of 1 mM, for 30 min using the perfusion method described above, before the application of the DAF-FM DA staining solution. All image acquisition parameters, including laser power, gain, offset, and exposure time, were kept strictly identical across all samples to ensure valid comparisons.

Callose deposition visualization

Callose deposition was visualized in the roots of 5-day-old seedlings following a 6-h. exposure to *Pst* DC3000 mVOCs, as this tissue is the primary site of the reported RSA remodeling. While leaves were also screened during initial experiments, the callose quantification presented in Fig. 3 focuses exclusively on the root elongation and differentiation zones where the K^+-dependent signaling occurs. Control seedlings were exposed to 10 mM $MgCl_2$ buffer in the same headspace co-cultivation system. Following the staining protocol with aniline blue solution (Hauck et al., 2003), tissues from *A. thaliana* Col-0 and the *fls2, pmr4*, and *pdko3* mutants were fixed in an ethanol:acetic acid (3:1, v/v) solution and subsequently stained with 0.01% (w/v) aniline blue in 150 mM K_2HPO_4 (pH 9.5). For the pharmacological inhibition of K+ fluxes as shown in Fig. 3, Col-0 seedlings were pre-incubated with 20 mM K^+ channel blocker tetraethylammonium chloride (TEA^+) for 1 h prior to mVOC exposure. Callose fluorescence in roots and leaves of *A. thaliana* Col-0 and the *fls2, pmr4*, and *pdko3* mutants was visualized using a fluorescence microscope (Nikon, Tokyo, Japan) equipped with a 10× objective under ultraviolet light.

Elicitor and pharmacological treatments

The flg22 peptide (QRLSTGSRINSAKDDAAGLQIA), corresponding to the conserved N-terminal fragment of bacterial flagellin, was purchased from Sigma-Aldrich (Milan, Italy). A 10 mM stock solution was prepared in sterile deionized water and stored at −20 °C. For experimental treatments, the stock was diluted to a final concentration of 10 μM in liquid half-strength MS medium. Seedlings were treated with 10 μM flg22 for the time intervals indicated in the figure legends (e.g., 30 min to 6 h) to serve as a positive control for FLS2-dependent signaling and protein accumulation.

Analysis of GUS and GFP reporter genes expression

To assess GUS reporter accumulation following exposure to *Pst* mVOCs, roots and leaves from both Col-0 and mutants were subjected to a 2-h incubation at 37 °C in a GUS staining solution. This incubation was performed at two distinct time points: 1 and 16 h after the initiation of *Pst* mVOC exposure. The staining buffer comprised 10 mM EDTA, 0.1% Triton X-100, 2 mM $K_3[Fe(CN)_6]$, 2 mM $K_4[Fe(CN)_6]$, and 1 mg/mL X-Gluc, all within a 50 mM NaH_2PO_4 buffer at pH 7.0 (Dedow et al., 2022). Stained samples were observed and photographed with a microscope

(Nikon). GFP analyses were performed with the Nikon Eclipse C1 confocal microscope. GFP fluorescence was imaged in a channel setting with 488 nm for GFP excitation (508 nm) and a channel for chlorophyll excitation (620 nm). For the quantification of GUS staining and fluorescence intensity, all images within an experimental set were acquired using identical settings. Fluorescence intensity was quantified in ImageJ from a defined region of interest (ROI) by measuring the mean gray value; n = 5 independent biological replicates per treatment unless otherwise specified in the figure legend.

qPCR analyses

Quantitative PCR (qPCR) was performed on a QuantStudio 3 Real-Time PCR System (Applied Biosystems, CA) to analyze gene expression in Arabidopsis Col-0 and the three mutant lines. Relative expression was calculated by comparing *Pst* DC3000 mVOC-exposed seedlings to untreated control seedlings grown under identical conditions in the headspace co-cultivation (HSCC) system without bacterial inoculation. Each 25 µL reaction contained 50–100 ng of cDNA template and Maxima SYBR Green/ROX qPCR Master Mix Kit (Thermo Fisher Scientific, USA). The two-step thermal profile for amplification involved an initial incubation at 50 °C for 2 min, denaturation at 95 °C for 10 min, followed by 40 cycles of 95 °C for 15 s and 60 °C for 60 s. Primers were designed using Primer 3 software (Table S1), with calculated amplification efficiencies ranging from 94 to 102% and correlation coefficients (R^2) exceeding 0.98. Cycle threshold (C_t) values were determined using the QuantStudio Design & Analysis software (Applied Biosystems, California). For normalization, the expression stability of three reference genes [*ACT2* (At3g18780), *eEF1Bα2* (At5g19510), and *UBP6* (At1g51710)] was evaluated across all experimental conditions. *UBP6* was determined to be the most stable reference gene (mean C_t variance < 0.2 cycles between treatments) and was used to calculate relative transcript abundance via the $2^{-\Delta\Delta Ct}$ method. The primers for these reference genes, as well as the target genes *AXR1, PIN1, PIN2*, and *PIN3*, are detailed in Supplementary Table S2. The analysis involved five independent biological replicates per treatment, with each sample analyzed in three technical replicates. To ensure amplification specificity, a melting curve analysis was performed at the end of each run, confirming a single peak for all targeted genes. Primer amplification efficiencies ranged from 94 to 102% with $R^2 > 0.98$.

Statistical analysis

Data were analyzed using Systat 10 (Systat Software, Inc.). For comparisons between multiple groups or treatments, a One-way or Two-way Analysis of Variance (ANOVA) was performed as appropriate for the experimental design. When significant differences were detected, Tukey's Honestly Significant Difference (HSD) post hoc test was employed for pairwise comparisons of means. All results are presented as the mean ± standard deviation (SD), and differences were considered statistically significant at $p < 0.05$. The specific number of biological replicates (independent experimental runs) and technical replicates for each data set are detailed in the corresponding figure legends and method subsections.

Results

Pst DC3000 mVOCs markedly remodel A. thaliana root system architecture without impacting leaf area

Exposure to *Pst* DC3000 mVOCs in the headspace co-cultivation (HSCC) system triggered pronounced remodeling of *A. thaliana* root system architecture (RSA). Control seedlings developed a typical primary root with numerous lateral branches (Fig. 1A), whereas plants exposed to the bacterial volatile blend displayed a markedly altered root phenotype (Fig. 1B). Primary root elongation was reduced by ~ 50%

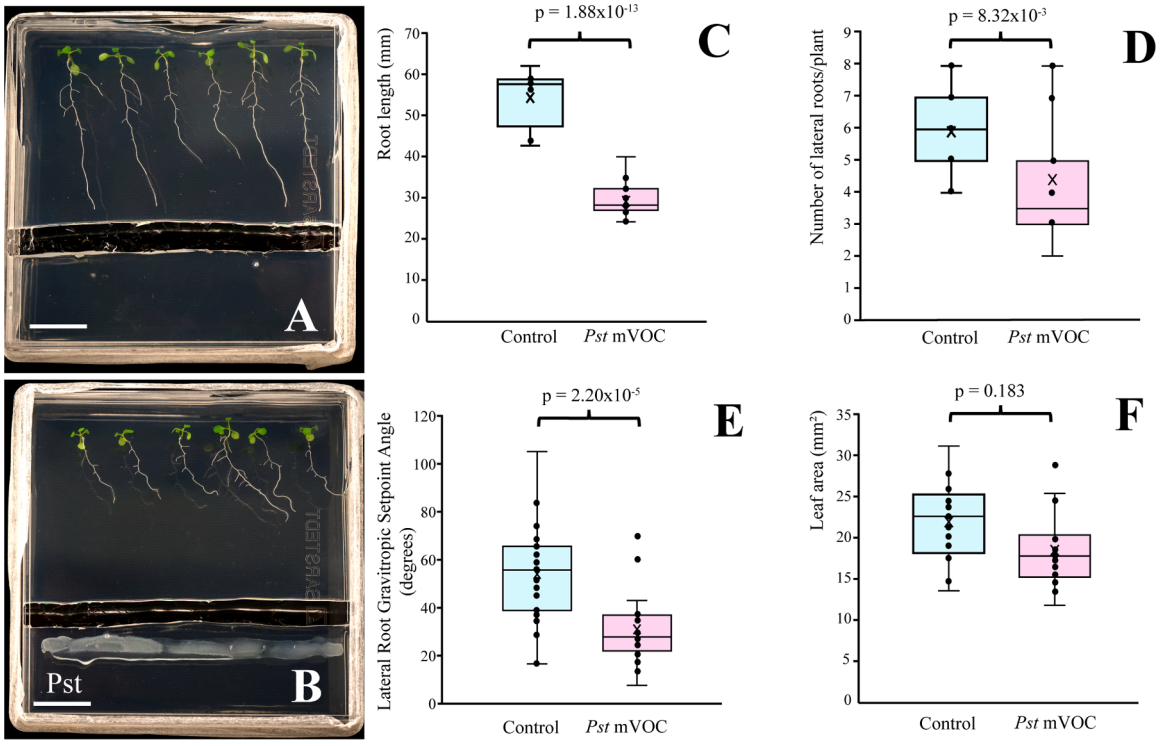

Fig. 1. Effects of *Pst* DC3000 mVOCs on *A. thaliana* root system architecture and leaf area. (**A**) Representative control seedlings in the headspace co-cultivation (HSCC) system. (**B**) Representative seedlings exposed to *Pst* DC3000 mVOCs. (**C**) Primary root length. (**D**) Number of lateral roots per seedling. (**E**) Lateral root gravitropic setpoint angle (LRGSA). (**F**) Total leaf area. n = 25 seedlings per treatment. Error bars represent standard deviation; "X" indicates the mean value. Scale bar = 20 mm.

relative to controls (Fig. 1C). The number of lateral roots decreased by about 40%, and the lateral root gravitropic setpoint angle (LRGSA) was reduced by nearly half, resulting in more downward-oriented lateral roots (Fig. 1D, E). Total leaf area remained unchanged (Fig. 1F), indicating that shoot growth was largely unaffected under these conditions and that the concentration of volatiles used is sub-toxic.

Pst DC3000 mVOCs trigger rapid, organ-specific Ca^{2+}, K^+, ROS and NO signaling that is differentially impaired in fls2 and pdko3 mutants

Rapid signaling events triggered by *Pst* DC3000 mVOCs were characterized by monitoring cytosolic Ca^{2+}, ligand- and voltage-gated K^+ channel activity, steady state H_2O_2 and NO production in shoots and roots of Col-0, *fls2*, and *pdko3* plants using fluorescent probes and indicator dyes (Fig. 2). In wild type (Col-0), *Pst* DC3000 mVOC exposure induced distinct temporal patterns in shoots and roots. Cytosolic Ca^{2+} increased strongly in shoots at 1 h, whereas roots showed only a modest rise at 2–3 h, indicating a weaker and delayed Ca^{2+} response belowground. Both ligand-gated and voltage-gated K^+ channels were rapidly activated, with clear increases detectable at 30 min and 1 h in both organs. H_2O_2 increased during the early phase, whereas NO peaked later, reaching a maximum at 6 h before declining at later time points.

Early signaling dynamics were substantially altered in *fls2*. Calcium elevations were stronger than in Col-0, especially in roots at 30 min, 2 h, and 3 h. In contrast, K^+ channel activation was markedly delayed. While Col-0 plants showed early activation at 30 min–1 h, the *fls2* mutant displayed its strongest K^+ reporter responses only at 3 h. H_2O_2 production was completely abolished in *fls2* throughout the time course, demonstrating a requirement for FLS2-associated signaling for ROS accumulation under volatile exposure.

Similarly, NO accumulation was strongly delayed. Col-0 plants exhibited a prominent NO peak at 6 h, whereas *fls2* showed no early NO increase, with a clear induction appearing only at 24 h, most pronounced in shoots.

Early signaling was even more strongly suppressed in *pdko3*, lacking PDLP1/2/3. Ca^{2+} elevations and H_2O_2 accumulation were almost completely absent, indicating that plasmodesmal function contributes critically to early Ca^{2+}- and ROS-associated responses to mVOCs. NO levels were also strongly reduced during the early phase (30 min–6 h), with a gradual increase observed only at 16–24 h, and only in shoots.

Despite these severe impairments, both ligand-gated and voltage-gated K^+ channels remained responsive, showing early activation at 30 min, although with altered temporal profiles relative to Col-0.

This selective preservation of K^+ signaling indicates that while early K^+ fluxes operate as an independent triggering branch, they must interact with PDLP-dependent Ca^{2+}, ROS, and NO to execute the full, integrated signaling program required for RSA remodeling. This hierarchical organization suggests that ionic triggers and redox coordination are functionally coupled via the plasmodesmatal network.

Pst DC3000 mVOCs induce plasmodesmal callose deposition requires PMR4, PDLPs and K^+-dependent signaling

To assess whether *Pst* DC3000 mVOCs regulate plasmodesmal permeability, we examined callose deposition. Aniline blue staining showed strong callose deposition at plasmodesmata in Col-0 roots after *Pst* DC3000 mVOC exposure, consistent with rapid symplastic gating (Fig. 3). The *fls2* mutant retained a Col-0 callose response, confirming FLS2 independence. In contrast, the callose synthase mutant *pmr4* showed no detectable signal, while *pdko3* displayed greatly reduced callose. Pretreatment of Col-0 seedlings with the K^+ channel blocker TEA^+ substantially suppressed callose deposition. These results place

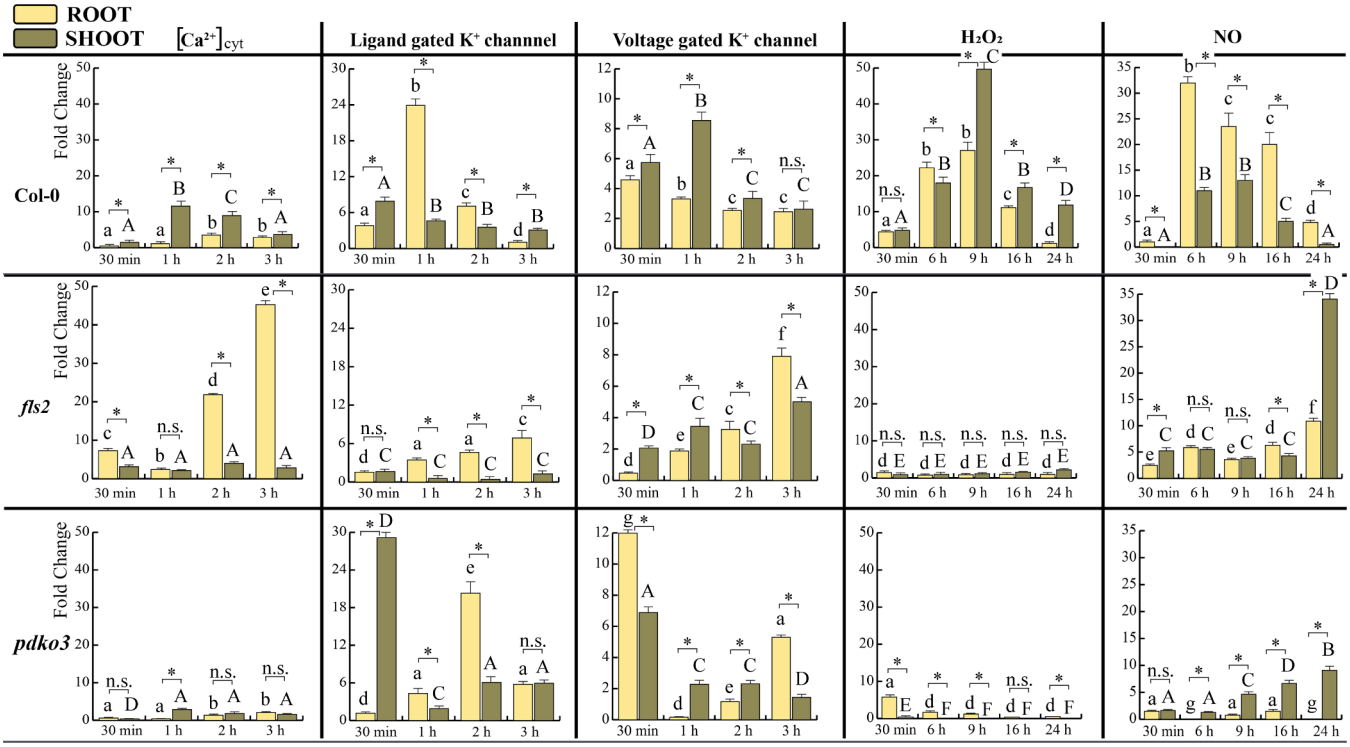

Fig. 2. Early ion and redox signalling responses to *Pst* DC3000 mVOCs in shoots and roots of *A. thaliana* Col-0, *fls2*, and *pdko3*. Fold-change in fluorescence intensity (relative to untreated controls) for cytosolic Ca^{2+}, ligand- and voltage-gated K^+ channel activity, H_2O_2 (ROS), and NO. Data are shown separately for shoots and roots across a 24-h time course. Bars represent standard deviation (n = 5 biological replicates). Y-axis scales are optimized for each signaling module to ensure visibility of significant trends across different biological magnitudes. Asterisks (*) indicate significant differences ($p < 0.05$, Tukey's HSD) between roots and shoots within each genotype and time point. Within the roots, different lowercase letters indicate significant differences ($p < 0.05$, Tukey's HSD); within the shoots, different uppercase letters express the same statistical difference. n.s., not significant differences ($p > 0.05$).

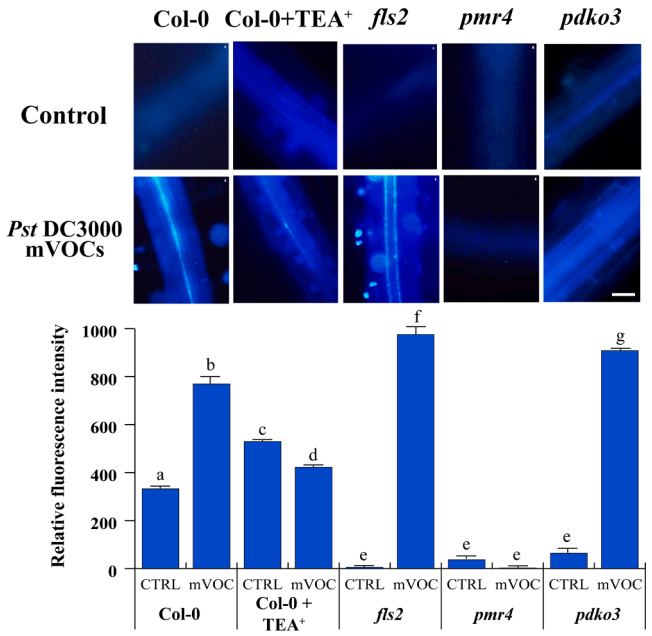

Fig. 3. *Pst* DC3000 mVOCs induce plasmodesmata-associated callose deposition in *A. thaliana* roots via a K⁺-, PDLP- and PMR4-dependent pathway. Representative aniline blue-stained roots of Col-0, *fls2, pmr4*, and *pdko3* seedlings under control and mVOC-treated conditions. Scale bar = 300 μm. Quantification of the relative fluorescence intensity (bottom bar graph) shows that mVOC exposure resulted in a significant increase in fluorescence intensity in Col-0 and in the mutants *fls2* and *pdko3*. Conversely, fluorescence was significantly reduced in Col-0 pre-treated with TEA^+. No significant changes were found in the *pmr4* mutant. Bars represent standard deviation (n = 5 biological replicates). Different letters indicate significant differences ($p < 0.05$, Tukey's HSD).

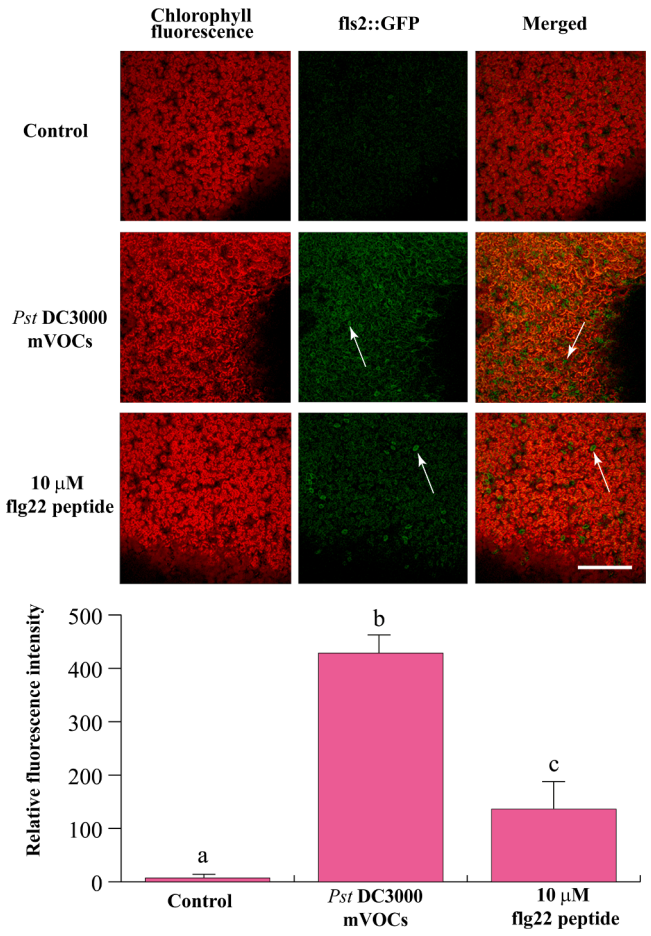

Fig. 4. *Pst* DC3000 mVOCs strongly upregulate *FLS2::GFP* abundance in *A. thaliana*. Confocal images of *FLS2::GFP* fluorescence in control plants, after exposure to *Pst* DC3000 mVOCs, and after treatment with 10 μM flg22 (a canonical FLS2 ligand). Enhanced signal is visible in stomatal guard cells (arrows) showing a stronger response to *Pst* DC3000 mVOCs than to flg22. Scale bars = 100 μm. Relative fluorescence intensity (bottom bar graph) shows a significant increase upon *Pst* DC3000 mVOC treatment. Bars represent standard deviation (n = 5 biological replicates). Different letters indicate significant differences ($p < 0.05$, Tukey's HSD).

early K^+ fluxes upstream of PDLP–PMR4-mediated callose synthesis and demonstrate that *Pst* DC3000 mVOCs close plasmodesmata through a K^+-dependent, PDLP/PMR4-dependent mechanism that bypasses FLS2.

Pst DC3000 mVOCs upregulate FLS2 receptor abundance

In *A. thaliana*, the leucine-rich repeat receptor kinase FLAGELLIN-SENSITIVE 2 (FLS2) acts as a PRR for the bacterial PAMP flagellin and contributes to resistance against bacterial pathogens (Zipfel et al., 2004). In *A. thaliana* plants expressing the flagellin receptor gene *FLS2::GFP*, exposure to *Pst* DC3000 mVOCs induced a significantly stronger fluorescence intensity compared to unexposed control *FLS2::GFP* plants. Fluorescence was particularly strong in stomatal guard cells which are the key entry points for bacterial pathogens and was primarily cytosolic in localization (Fig. 4). Surprisingly, the fluorescence intensity observed with *Pst* DC3000 mVOCs was higher than that observed in *A. thaliana FLS2::GFP* plants treated with 10 μM flg22 peptide, a well-characterized FLS2 elicitor (Jelenska et al., 2017). Similarly, with flg22, stomata showed the highest fluorescence intensity of FLS2 (Fig. 4)

Pst DC3000 mVOCs selectively induce transcriptional activation of PDLP2, PDLP3 and PDLP4

To investigate whether plasmodesmal regulatory genes are transcriptionally responsive to *Pst* DC3000 mVOCs, we monitored promoter activity of PDLP2, PDLP3, PDLP4 and PDLP5 using GUS reporter lines (Fig. 5). *PDLP2::GUS, PDLP3::GUS* and *PDLP4::GUS* exhibited clear induction after 3 h of volatile exposure, and this activation was maintained or further enhanced after 24 h, indicating a rapid and sustained transcriptional response. In contrast, the *PDLP5::GUS* reporter showed no detectable GUS activity under control or volatile-treated conditions, demonstrating that PDLP5 is unresponsive to mVOCs within the examined timeframe. These results show that PDLP2, PDLP3, and PDLP4, but not PDLP5, are transcriptionally responsive to bacterial volatiles and likely contribute to sustained plasmodesmatal regulation.

Pst DC3000 mVOCs reconfigure the auxin transport apparatus and signaling response

To assess how *Pst* DC3000 mVOCs influence auxin signaling, we examined a panel of GUS-based reporters (Fig. 6). The synthetic auxin-responsive reporter *DR5::GUS* showed increased staining at the root tip after volatile exposure, with the strongest signal at 16 h, consistent with elevated auxin-responsive transcription under mVOCs. By contrast, *DR5::GUS* in *axr1* background (*axr1 DR5::GUS*), in which SCF–TIR1/AFB-mediated auxin signaling is genetically attenuated, showed no detectable treatment-dependent change. Together, these data suggest that the mVOC-induced DR5 response requires an intact AXR1-dependent signaling capacity and/or is largely confined to the canonical SCF-TIR1/AFB transcriptional pathway.

Auxin transport reporters exhibited distinct and opposing patterns. *PIN1::GUS* showed a transient induction after 1 h of mVOC exposure before returning to levels comparable to controls at later time points,

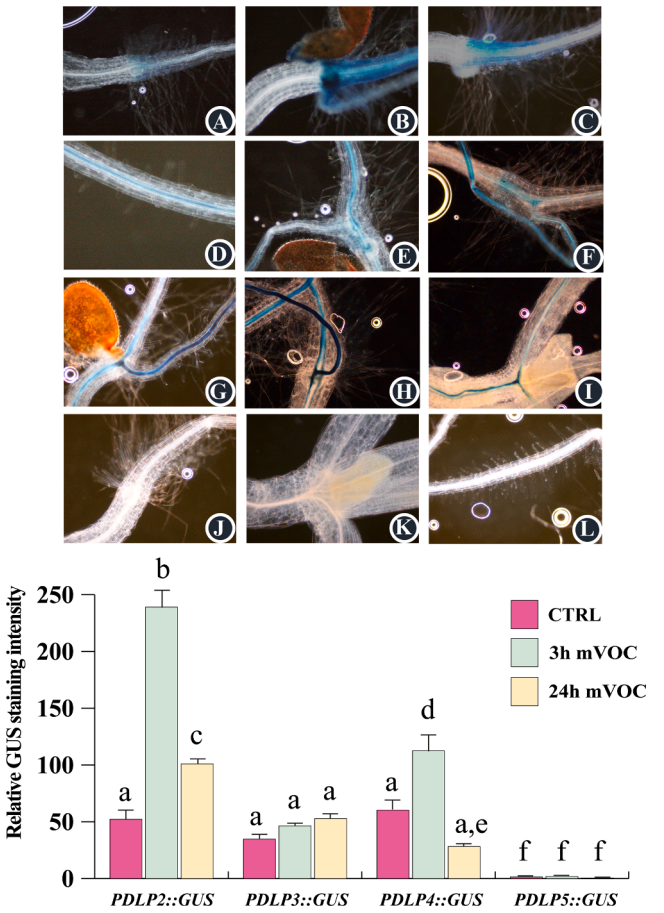

Fig. 5. *Pst* DC3000 mVOCs rapidly and selectively induce transcriptional activation of PDLP2, PDLP3, and PDLP4. GUS reporter expression driven by the PDLP2, PDLP3, PDLP4 and PDLP5 promoters in *A. thaliana* roots exposed to *Pst* DC3000 mVOCs. For each reporter line, untreated seedlings (control) are shown together with plants exposed to the volatile blend for 3 and 24 h. *PDLP2::GUS, PDLP3::GUS* and *PDLP4::GUS* displayed clear induction after 3 h of exposure, with promoter activity maintained or further increased at 24 h, indicating that these PD-associated regulators are rapidly transcriptionally activated by bacterial volatiles. In contrast, *PDLP5::GUS* showed no detectable GUS expression under any treatment, demonstrating that PDLP5 is not responsive to *Pst* mVOCs within the examined timeframe. (**A**) *PDLP2::GUS* control; (**B**) *PDLP2::GUS* exposed to mVOCs for 3 h; (**C**) *PDLP2::GUS* exposed to mVOCs for 24 h; (**D**) *PDLP3::GUS* control; (**E**) *PDLP3::GUS* exposed to mVOCs for 3 h; (**F**) *PDLP3::GUS* exposed to mVOCs for 24 h; (**G**) *PDLP4::GUS* control; (**H**) *PDLP4::GUS* exposed to mVOCs for 3 h; (**I**) *PDLP4::GUS* exposed to mVOCs for 24 h; (**J**) *PDLP5::GUS* control; (**K**) *PDLP5::GUS* exposed to mVOCs for 3 h; (**L**) *PDLP5::GUS* exposed to mVOCs for 24 h. Relative GUS staining intensity (lower bar graph). Different lowercase letters indicate significant ($p < 0.05$, Tukey's HSD) differences.

indicating a short-lived increase in basal auxin efflux capacity. Conversely, *PIN3::GUS* displayed a strong and consistent reduction in GUS accumulation across all examined time points, consistent with suppression of PIN3-mediated auxin redistribution. These findings demonstrate that *Pst* DC3000 mVOCs do not uniformly activate auxin signaling but rather trigger selective transcriptional enhancement of DR5, transient activation of PIN1, and stable repression of PIN3, helping to reconfigure auxin transport and signaling during the early root response to bacterial volatiles.

Pst DC3000 mVOCs induce distinct temporal transcriptional dynamics of PIN and AXR1 genes

To examine how *Pst* DC3000 mVOCs influence auxin transporter

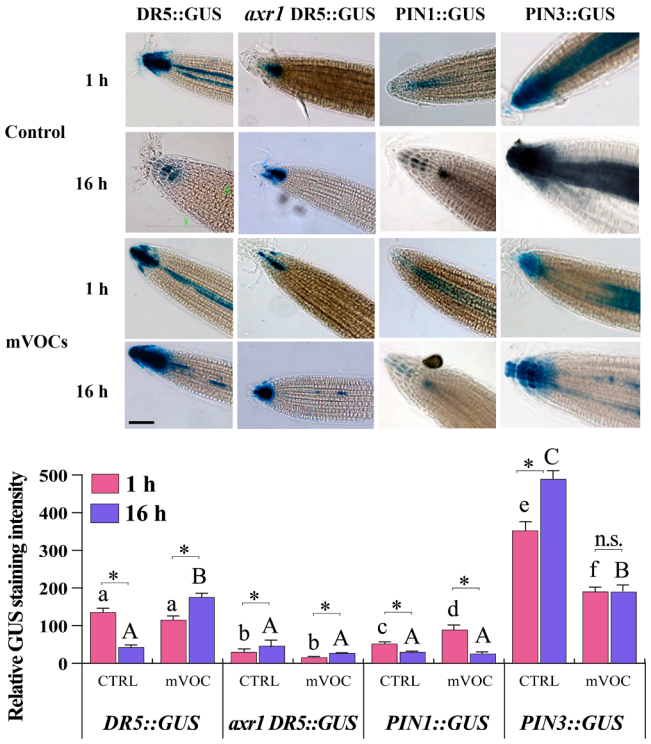

Fig. 6. *Pst* DC3000 mVOCs reprogram auxin signaling and polar transport reporters in *A. thaliana*. GUS reporter accumulation in *DR5::GUS, axr1 DR5::GUS, PIN1::GUS* and *PIN3::GUS* seedlings exposed to *Pst* DC3000 mVOCs for the indicated times. The synthetic auxin-responsive reporter *DR5::GUS* showed enhanced staining at the root tip after mVOC exposure (strongest at 16 h), whereas *axr1 DR5::GUS* did not display significant differences compared to controls. The auxin efflux carrier reporter *PIN1::GUS* exhibited a transient induction after 1 h of exposure before returning to basal levels, while *PIN3::GUS* displayed a consistent reduction in GUS accumulation across all examined time points upon *Pst* DC3000 mVOC exposure. Scale bar = 500 µm. Relative GUS staining intensity (lower bar graph). Asterisks (*) indicate significant differences ($p < 0.05$, Tukey's HSD) between 1 and 16 h exposure. Different lowercase letters indicate significant ($p < 0.05$, Tukey's HSD) differences at 1 h. exposure, whereas different capital letters indicate significant differences ($p < 0.05$, Tukey's HSD) at 16 h. exposure. n.s., not significant ($p > 0.05$) differences.

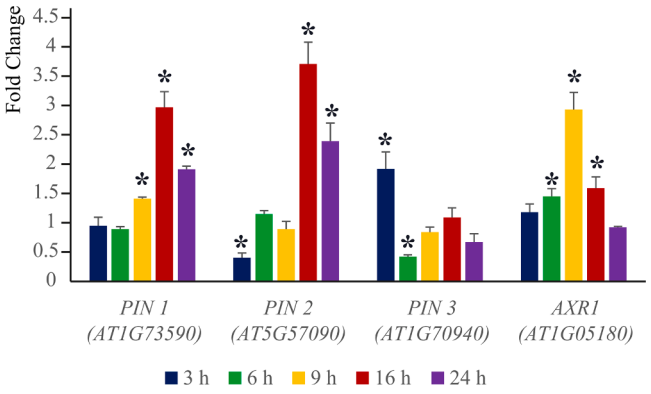

Fig. 7. Temporal transcriptional dynamics of auxin transport and signalling genes in *A. thaliana* seedlings exposed to *Pst* DC3000 mVOCs. Relative transcript levels (fold-change versus untreated controls grown without bacterial exposure) of *PIN1, PIN2, PIN3* and *AXR1* were quantified in *A. thaliana* seedlings exposed to *Pst* DC3000 mVOCs over the indicated time course. Error bars represent standard deviation (n = 5 biological replicates), asterisk indicates significant ($p < 0.05$) differences with respect to control.

gene expression, we quantified transcript levels of *PIN1, PIN2, PIN3*, and *AXR1* over a 24 h time course (Fig. 7) relative to untreated control seedlings grown in the same headspace co-cultivation (HSCC) system without the presence of *Pst* DC3000. *PIN1* expression remained unchanged during the early phase (3–6 h), but became upregulated from 9 h onwards, with elevated transcript levels maintained through 16–24 h. *PIN2* displayed a biphasic pattern: transcripts were reduced to less than half of control levels at 3 h, recovered by 6–9 h, and then became strongly upregulated at 16 h and 24 h (approximately 3.5-fold and 2.5-fold, respectively).

PIN3 exhibited a brief and modest induction at 3 h, likely representing a short transient response that was not captured by the *PIN3::GUS* reporter, followed by reduced expression at 6 h and no sustained upregulation at later time points. This overall pattern supports a general downregulation of *PIN3*, consistent with the suppression observed in reporter analyses at the later stages. *AXR1* transcript levels remained close to baseline during the early points but showed a marked transient induction at 9 h (~3-fold), returning towards baseline thereafter.

Together, these patterns corroborate the reporter data and reveal that *Pst* DC3000 mVOCs induce distinct and temporally resolved transcriptional responses among auxin transport and signaling genes, characterized by late induction of *PIN1* and *PIN2*, rapid repression of *PIN3*, and a transient mid-term activation of *AXR1*.

Synthetic 2-methylbutanoic acid partially recapitulates Pst DC3000 mVOC-induced root architecture and leaf area changes

Previous work identified 2-methylbutanoic acid (2-MBA) as a major bacterium-specific component of the *Pst* DC3000 volatile blend using headspace GC–MS analysis (Paponov et al., submitted; Supplemental Table S1). To test its contribution to the root architectural changes described above, we exposed seedlings to synthetic 2-MBA under the same growth conditions. After 14 days, 2-MBA significantly reduced primary root length and the number of lateral roots per plant and decreased the lateral root gravitropic setpoint angle, while total leaf area remained unchanged (Fig. 8). The direction of these changes was qualitatively similar but generally weaker than the phenotype elicited by the full *Pst* DC3000 volatile blend (cf. Figs. 1 and 8). These observations support a contribution of 2-MBA to volatile-induced root system remodeling but also indicate that additional volatile components and/or interactions are required to fully reproduce the mVOC phenotype. A more detailed dissection of 2-MBA–specific effects on root architecture will therefore require dedicated future studies.

Discussion

Plants, as sessile organisms, have evolved sophisticated mechanisms to detect microbial cues and rapidly adjust development and immunity. Microbial VOCs serve as diffusible, long-range signals that mediate inter- and intra-kingdom communication, modulating plant growth, RSA and defense (Chandrasekaran et al., 2023; Schulz-Bohm et al., 2017; Weisskopf et al., 2021). Here we demonstrate that mVOCs emitted by *Pseudomonas syringae* pv. *tomato* DC3000 (*Pst* DC3000) trigger extensive RSA remodeling in *A. thaliana* while activating a coordinated cascade of early ion/redox signaling, plasmodesmatal gating and auxin-transport reprogramming. The bacterial volatile blend contains 2-methylbutanoic acid (2-MBA), a known bacterial catabolite (Beck et al., 2002), which alone recapitulates the core direction of the RSA response, although with reduced magnitude, indicating that additional volatiles and/or synergistic interactions are required for the full developmental output. A central finding of this study is the non-canonical involvement of the FLS2 receptor in the response to *Pst* DC3000 mVOCs. While FLS2 is established as the PRR for the bacterial peptide flg22, our results demonstrate that it also plays a critical role in

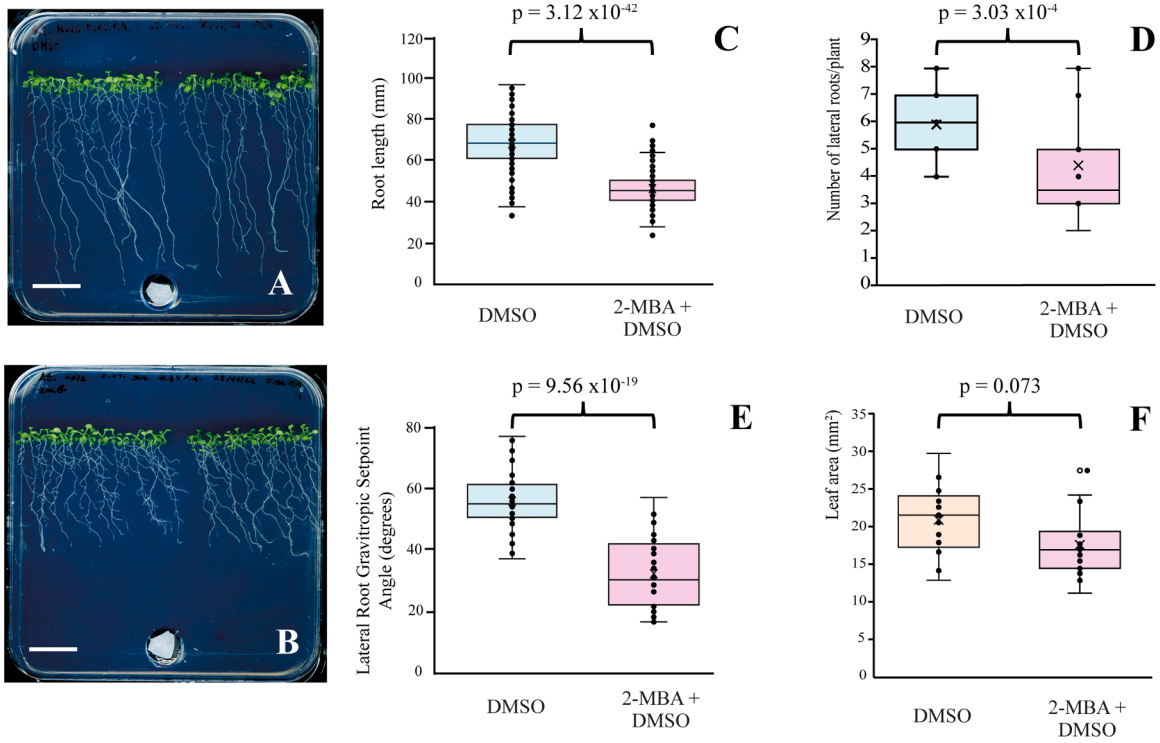

Fig. 8. Synthetic 2-methylbutanoic acid (2-MBA) partially recapitulates *Pst* DC3000 mVOC-induced changes in *A. thaliana* root system architecture and leaf area. (**A**) Representative DMSO-treated control seedlings. (**B**) Representative seedlings treated with 2-MBA dissolved in DMSO. (**C**) Primary root length. (**D**) Number of lateral roots per seedling. (**E**) Lateral root gravitropic setpoint angle (LRGSA). (**F**) Total leaf area. Seedlings were grown for 14 days under the same HSCC conditions used for mVOC assays. n = 75 seedlings per treatment. Y-axis scales are optimized with respect to Fig. 1 to ensure visibility of significant trends across different biological magnitudes. Error bars represent standard deviation; "X" indicates the mean value. Changes occur in the same direction as the full *Pst* DC3000 mVOC blend (cf. Fig. 1) but with lower magnitude.

the volatile-triggered signaling cascade. Specifically, *fls2* mutants failed to mount the early ROS burst and exhibited significantly delayed NO production upon volatile exposure.

The ecological significance of altered root morphology and a growth-defense trade-off

Changes in RSA upon *Pst* DC3000 mVOC perception, particularly reduced lateral root number and altered LRGSA, directly reshape how the root system occupies soil space. A reduced LRGSA in our system corresponds to more downward/steeper lateral root growth, which is expected to influence soil exploration patterns and potentially alter access to water and nutrients across soil layers (Guo et al., 2024). Because *Pst* DC3000 can colonize *A. thaliana* roots and cause disease despite its primary foliar lifestyle (Lakshmanan et al., 2012), these architectural shifts may be interpreted as a belowground anticipatory defence strategy. The observed changes are suggestive of a growth–defense trade-off, whereby resource allocation to growth might be curtailed to accommodate the activation of immune and symplastic modules (Figueroa-Macías et al., 2021; He et al., 2022; Guo et al., 2024). This provides a biological reason for the plant to slow its roots (saving energy for defense and altering its trajectory to avoid the pathogen) without dying from toxic exposure. Volatile perception could potentially function as an early-warning system that translates microbial risk into rapid signalling and structural reconfiguration, potentially minimising future exposure and prioritising defence over expansion

Pst DC3000 mVOCs engage PRR-associated signaling modules and activate downstream responses

Exposure to *Pst* DC3000 mVOCs triggers a multi-layered response that includes rapid ion fluxes and redox-associated signaling, mirroring the early signaling logic of pattern-triggered immunity even though mVOCs are chemically distinct from classical PAMPs. The early Ca^{2+} dynamics and ROS-related outputs we observed are consistent with canonical early events downstream of cell-surface immune receptors, where Ca^{2+} transients and ROS bursts function as organizing nodes for downstream defense responses (DeFalco and Zipfel, 2021; Köster et al., 2022). The overlap in early signaling logic demonstrates that volatile cues can feed into established immune-signaling architectures.

FLS2 as a temporal coordinator of Pst DC3000 mVOC-triggered signaling

Although FLS2 is canonically the receptor for bacterial flagellin (flg22) (Zipfel et al., 2004), our data reveal that its strong influence on mVOC-triggered outputs suggests that it may act more broadly as a signaling hub or temporal coordinator. In this model, the volatile perception, that is likely mediated by yet unidentified primary sensors, converges on the FLS2-BAK1 complex to modulate the execution of the oxidative burst. This is supported by our observation that in the absence of FLS2 signaling becomes asynchronous: the early H_2O_2 burst was abolished and NO induction delayed, while root Ca^{2+} elevations were enhanced and K^+ channel activation postponed, pointing to disrupted homeostatic coordination. This decoupling shows that FLS2 is required to translate initial Ca^{2+} signatures into timely redox and ionic outputs (DeFalco and Zipfel, 2021; Mersmann et al., 2010). We argue that this hub function might allow the plant to integrate volatile warning cues into a coherent physiological response, ensuring that the downstream symplastic gating and auxin-transport reconfiguration are executed within a specific developmental window to successfully remodel the root system.

Plasmodesmal function in early signal propagation and response integration

The *pdko3* (pdlp1/2/3) mutant almost completely suppressed Ca^{2+} elevations, H_2O_2 accumulation and early NO production, yet preserved K^+ channel activity, highlighting a crucial role for plasmodesmata-localized proteins (PDLPs) in the volatile-triggered signaling program. These results indicate that an intact PDLP-dependent plasmodesmatal network is essential for signal amplification and cell-to-cell propagation of most early responses, but that K^+ fluxes constitute a partially independent branch (Bricchi et al., 2013; Tee and Faulkner, 2024). Late NO increases observed in shoots of both mutants further suggest that NO can be generated through multiple, partially redundant routes whose specificity depends on timing, localization and amplitude (Wendehenne et al., 2004).

The PDLP-PMR4 axis in symplastic gating with K^+ signaling as a required upstream component

Volatile-induced callose deposition at plasmodesmata occurred normally in *fls2* but was abolished in *pmr4* and strongly reduced in *pdko3*, demonstrating that symplastic gating proceeds via a PDLP–PMR4-dependent pathway that is independent of FLS2. Pharmacological blockade of K^+ channels with TEA^+ prevented callose formation in Col-0 roots, placing K^+ fluxes upstream of PDLP–PMR4-mediated callose synthesis. While Ca^{2+} is often implicated in plasmodesmatal regulation (Zanini and Burch-Smith, 2024), our data highlight K^+ signaling as the critical early trigger that enables execution of PDLP/PMR4-dependent closure under volatile exposure (Ellinger et al., 2013; Saatian et al., 2023; Lee et al., 2011a; Tee and Faulkner, 2024). Rapid and selective transcriptional induction of PDLP2, PDLP3 and PDLP4 (but not PDLP5) provides a mechanism for sustained symplastic control. The lack of PDLP5 induction suggests that volatile-triggered gating recruits a specific PDLP subset distinct from SA-associated defense modules (Lee et al., 2011b), allowing fine-tuned symplastic isolation without full immune engagement.

The interaction between these early signals constitutes a hierarchical framework for volatile-induced root remodeling. In this model, rapid K^+ fluxes act as the primary structural trigger, initiating the PDLP-PMR4-dependent callose deposition that executes symplastic gating. Simultaneously, Ca^{2+} transients and the FLS2-dependent H_2O_2 burst function as a temporal regulator, ensuring that these cellular responses are synchronized and correctly timed. The *pdko3* mutant, which preserves K^+ fluxes but suppresses Ca^{2+}, H_2O_2, and early NO signatures, highlights that PDLPs are essential not only for gating but for the amplification and cell-to-cell propagation of these interacting signals. Ultimately, this integrated ion/redox/symplastic circuit converges on the auxin transport apparatus, where the resulting cellular isolation and redox environment facilitate the sustained repression of PIN3 and the reprogramming of root architecture.

Reconfiguring the auxin transport apparatus

Pst DC3000 mVOCs enhanced *DR5::GUS* accumulation at the root tip in an AXR1-dependent manner while triggering opposing changes in PIN reporters: transient *PIN1* induction and stable *PIN3* repression. qRT-PCR confirmed late upregulation of *PIN1* and *PIN2*, transient *AXR1* induction and sustained *PIN3* downregulation. These patterns are consistent with canonical auxin signaling feeding back on *PIN* expression (Ulmasov et al., 1997; Vieten et al., 2005; del Pozo et al., 2002) and with reduced PIN3-mediated auxin redistribution, which can shift the balance of gravitropic versus anti-gravitropic fluxes to produce the observed steeper LRGSA (Friml et al., 2002; Rahman et al., 2010; Waidmann et al., 2019; Roychoudhry et al., 2023). Thus, auxin-transport reprogramming provides a direct mechanistic link between early signaling and long-term RSA remodeling. While protein abundance is a strong proxy for transport capacity in roots, future studies using radiolabeled auxin could further quantify the specific flux rates.

The major volatile 2-methylbutanoic acid establishes the core developmental response to Pst DC3000

Synthetic 2-MBA reproduced the directional changes in primary root length, lateral root number and LRGSA, although with lower magnitude than the complete blend. Specifically, while 2-MBA alone accounts for approximately 70% of the primary root inhibition observed with the full volatile blend, the complete phenotypic strength requires the presence of the full *Pst* DC3000 mixture. This suggests a synergistic interaction where 2-MBA establishes the core direction of the RSA response, while other blend components, likely acting in concert through parallel signaling modules, amplify the magnitude of the structural remodeling. This partial recapitulation aligns with the known capacity of microbial volatiles to inhibit growth and reshape RSA (Bitas et al., 2013). The sustained *PIN3* repression observed with the complete blend offers a plausible route by which the mixture fine-tunes the anti-gravitropic offset that normally maintains non-vertical lateral root growth (Roychoudhry et al., 2023).

Limitations and future perspectives

Several limitations of the present study should be acknowledged. (i) The primary receptors for *Pst* DC3000 volatiles remain to be identified; our genetic and pharmacological data establish functional necessity for FLS2, K+ channels, PDLPs and PMR4, but not the upstream sensing step. (ii) Our analyses report *PIN* expression, promoter activity and protein abundance, but not auxin transport rates directly; functional reprogramming of polar auxin transport thus remains to be confirmed, for example by radio-labelled IAA flux assays or DII-VENUS quantification. (iii) Although our genetic and pharmacological data are mutually consistent, formal epistasis (e.g., *pmr4 pdko3* or *fls2 pdko3* double mutants) was not performed and the proposed signaling order should be regarded as a working model. (iv) The bioactivity of 2-MBA was tested as a single compound; combinatorial assays with other major volatile components, dose–response curves and disease-resistance phenotyping after volatile pre-exposure remain to be carried out. (v) Translating the present findings from the controlled headspace co-cultivation system to the heterogeneous chemical and physical environment of the soil rhizosphere represents an essential future challenge.

Conclusions

This work shows that *A. thaliana* roots actively reprogram their developmental trajectory in response to *Pst* DC3000 mVOCs. We identify a coordinated signaling framework in which early K^+ fluxes operate upstream of PDLP–PMR4-dependent plasmodesmatal closure, while FLS2 coordinates the timing of ROS and NO outputs without being required for symplastic gating. In parallel, *Pst* DC3000 mVOCs reconfigure auxin signaling and PIN-mediated transport, most notably through sustained *PIN3* repression, thereby driving reduced branching and steeper lateral root orientation. Furthermore, while 2-methylbutanoic acid emerges as a major bioactive component that establishes the core direction of RSA remodeling, full phenotypic strength requires the synergistic action of the complete *Pst* DC3000 volatile blend.

Together, these findings reveal how microbial volatiles are translated into integrated ion/redox, symplastic, and hormonal outputs that reshape root architecture as an anticipatory defense strategy (Fig. 9). Specific limitations and the next experimental priorities required to consolidate this model are discussed in the preceding 'Limitations and future perspectives' subsection.

Funding

This work was supported by a grant from the University of Turin research funds to M.E.M. (RILO2024) and by the Autonomous Province of Trento (Italy) to M.M.

Declaration of generative AI in scientific writing

During the preparation of this work, the author used Grok and DeepSeek to improve text clarity. After using this tool/service, the authors reviewed and edited the content as needed and take full responsibility for the content of the published article.

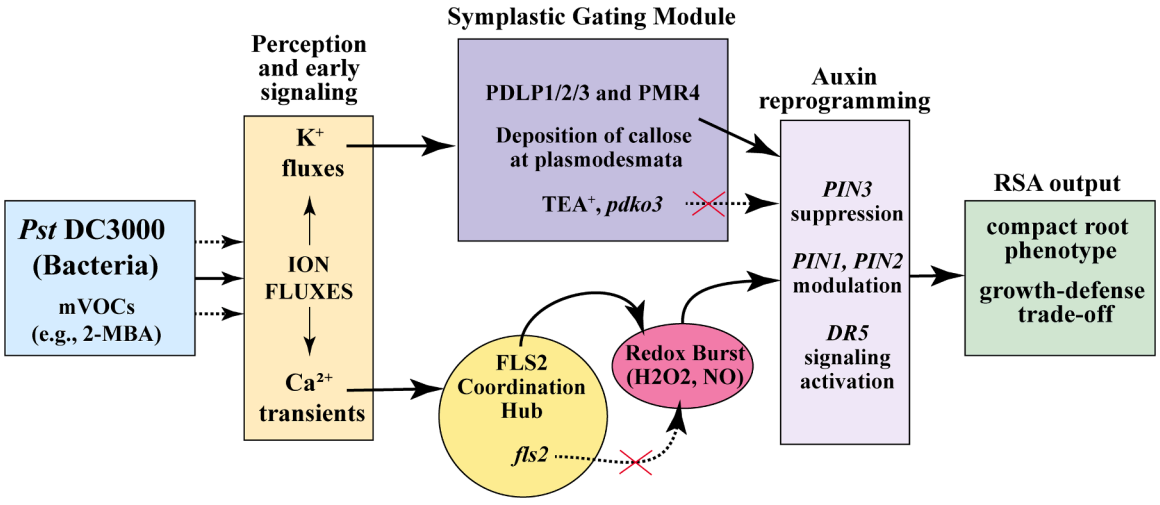

Fig. 9. Proposed model for *Pst* DC3000 mVOC-induced root system architecture (RSA) remodeling. The schematic illustrates the integrated signaling network through which microbial volatiles (mVOCs), specifically 2-methylbutanoic acid (2-MBA), reprogram *A. thaliana* root development. Perception and early signaling: Exposure to the *Pst* DC3000 volatile blend triggers rapid K^+ fluxes and cytosolic Ca^{2+} transients. Symplastic gating module: rapid K^+ fluxes operate upstream of PDLP1/2/3 and PMR4, driving the deposition of callose at plasmodesmata. This structural response executes symplastic gating, effectively isolating root cells to facilitate hormonal reprogramming. Blockade of K^+ channels with TEA^+ or loss of PDLPs (*pdko3*) disrupts this gating mechanism. The FLS2 Coordination Hub: FLS2 acts as a temporal coordinator, integrating early signals to activate the timely production of H_2O_2 and NO. Genetic loss of FLS2 uncouples these redox bursts from the initial ion signatures. Hormonal reprogramming: the integrated ion, redox, and symplastic signals converge on the auxin transport apparatus, leading to the sustained repression of *PIN3*, modulation of *PIN1* and *PIN2*, and transcriptional activation of DR5-mediated signaling. RSA output: These molecular shifts drive the observed compact root phenotype, characterized by inhibited primary root elongation, reduced lateral branching, and a steeper (downward) gravitropic setpoint angle. This remodeling represents an anticipatory defense strategy to minimize pathogen exposure through a growth-defense trade-off.

CRediT authorship contribution statement

Chidananda Nagamangala Kanchiswamy: Writing – review & editing, Writing – original draft, Visualization, Validation, Supervision, Methodology, Investigation, Formal analysis, Data curation, Conceptualization. **Ivan A. Paponov:** Writing – review & editing, Writing – original draft, Visualization, Validation, Supervision, Methodology, Investigation, Formal analysis, Data curation, Conceptualization. **Mickael Malnoy:** Writing – review & editing, Resources, Methodology, Data curation, Conceptualization. **Francesco Caldo:** Writing – review & editing, Investigation, Formal analysis. **Suruchi Roychoudhry:** Writing – review & editing, Methodology, Investigation, Formal analysis, Data curation, Conceptualization. **Massimo E. Maffei:** Writing – review & editing, Writing – original draft, Validation, Supervision, Resources, Project administration, Methodology, Investigation, Funding acquisition, Formal analysis, Data curation, Conceptualization.

Declaration of competing interest

The authors declare that they have no known competing financial interests or personal relationships that could have appeared to influence the work reported in this paper.

Supplementary materials

Supplementary material associated with this article can be found, in the online version, at doi:10.1016/j.stress.2026.101438.

Data availability

Data will be made available on request.

References

Beck, H.C., Hansen, A.M., Lauritsen, F.R., 2002. Metabolite production and kinetics of branched-chain aldehyde oxidation in Staphylococcus xylosus. Enzyme Microb. Technol. 31, 94–101.

Bitas, V., Kim, H.S., Bennett, J.W., Kang, S., 2013. Sniffing on microbes: diverse roles of microbial volatile organic compounds in plant health. Mol. Plant Microbe Interact. 26, 835–843.

Bricchi, I., Occhipinti, A., Bertea, C.M., Zebelo, S.A., Brillada, C., Verrillo, F., De Castro, C., Molinaro, A., Faulkner, C., Maule, A.J., Maffei, M.E., 2013. Separation of early and late responses to herbivory in Arabidopsis by changing plasmodesmal function. Plant J. 73, 14–25.

Chandrasekaran, M., Paramasivan, M., Sahayarayan, J.J., 2023. Microbial volatile organic compounds: an alternative for chemical fertilizers in sustainable agriculture development. Microorganisms 11, 18.

Chen, L., Liu, Y., 2024. The function of root exudates in the root colonization by beneficial soil rhizobacteria. Biology (Basel) 13.

Dastidar, M.G., Jouannet, V., Maizel, A., 2012. Root branching: mechanisms, robustness, and plasticity. WIREs Dev. Biol. 1, 329–343.

Dedow, L.K., Oren, E., Braybrook, S.A., 2022. Fake news blues: a GUS staining protocol to reduce false-negative data. Plant Direct 6, 8.

Defalco, T.A., Zipfel, C., 2021. Molecular mechanisms of early plant pattern-triggered immune signaling. Mol. Cell 81, 3449–3467.

Del Pozo, J.C., Dharmasiri, S., Hellmann, H., Walker, L., Gray, W.M., Estelle, M., 2002. AXR1-ECR1-dependent conjugation of RUB1 to the Arabidopsis Cullin AtCUL1 is required for auxin response. Plant Cell 14, 421–433.

Ellinger, D., Naumann, M., Falter, C., Zwikowics, C., Jamrow, T., Manisseri, C., Somerville, S.C., Voigt, C.A., 2013. Elevated early callose deposition results in complete penetration resistance to powdery mildew in Arabidopsis. Plant Physiol. 161, 1433–1444.

Figueroa-Macías, J.P., García, Y.C., Núñez, M., Díaz, K., Olea, A.F., Espinoza, L., 2021. Plant growth-defense trade-offs: molecular processes leading to physiological changes. Int. J. Mol. Sci. 22.

Fincheira, P., Quiroz, A., 2018. Microbial volatiles as plant growth inducers. Microbiol. Res. 208, 63–75.

Friml, J., Wiśniewska, J., Benková, E., Mendgen, K., Palme, K., 2002. Lateral relocation of auxin efflux regulator PIN3 mediates tropism in Arabidopsis. Nature 415, 806–809.

Garbeva, P., Weisskopf, L., 2020. Airborne medicine: bacterial volatiles and their influence on plant health. New Phytol. 226, 32–43.

Gifford, M.L., Xu, G., Dupuy, L.X., Vissenberg, K., Rebetzke, G., 2024. Root architecture and rhizosphere–microbe interactions. J. Exp. Bot. 75, 503–507.

Guo, C., Bao, X., Sun, H., Chen, J., Zhu, L., Zhang, J., Zhang, H., Zhang, Y., Zhang, K., Bai, Z., Li, A., Liu, L., Li, C., 2024. The crucial role of lateral root angle in enhancing drought resilience in cotton. Front. Plant Sci. 15, 2024.

Hauck, P., Thilmony, R., He, S.Y., 2003. A Pseudomonas syringae type III effector suppresses cell wall-based extracellular defense in susceptible Arabidopsis plants. Proc. Natl. Acad. Sci. USA 100, 8577–8582.

He, Z., Webster, S., He, S.Y., 2022. Growth-defense trade-offs in plants. Curr. Biol. 32, R634–R639.

Jelenska, J., Davern, S.M., Standaert, R.F., Mirzadeh, S., Greenberg, J.T., 2017. Flagellin peptide flg22 gains access to long-distance trafficking in Arabidopsis via its receptor, FLS2. J. Exp. Bot. 68, 1769–1783.

Kanchiswamy, C.N., Malnoy, M., Maffei, M.E., 2015. Bioprospecting bacterial and fungal volatiles for sustainable agriculture. Trends Plant Sci. 20, 206–211.

Kolupaev, Y.E., Karpets, Y.V., Dmitriev, A.P., 2015. Signal mediators in plants in response to abiotic stress: calcium, reactive oxygen and nitrogen species. Cytol. Genet. 49, 338–348.

Köster, P., Defalco, T.A., Zipfel, C., 2022. Ca(2+) signals in plant immunity. EMBO J. 41, e110741.

Lakshmanan, V., Kitto, S.L., Caplan, J.L., Hsueh, Y.-H., Kearns, D.B., Wu, Y.-S., Bais, H.P., 2012. Microbe-associated molecular patterns-triggered root responses mediate beneficial rhizobacterial recruitment in Arabidopsis. Plant Physiol. 160, 1642–1661.

Lee, J.-Y., Wang, X., Cui, W., Sager, R., Modla, S., Czymmek, K., Zybaliov, B., Van Wijk, K., Zhang, C., Lu, H., Lakshmanan, V., 2011a. A plasmodesmata-localized protein mediates crosstalk between cell-to-cell communication and innate immunity in Arabidopsis. Plant Cell 23, 3353–3373.

Lee, J.Y., Wang, X., Cui, W., Sager, R., Modla, S., Czymmek, K., Zybaliov, B., Van Wijk, K., Zhang, C., Lu, H., Lakshmanan, V., 2011b. A plasmodesmata-localized protein mediates crosstalk between cell-to-cell communication and innate immunity in Arabidopsis. Plant Cell 23, 3353–3373.

Lim, G.-H., Shine, M.B., De Lorenzo, L., Yu, K., Cui, W., Navarre, D., Hunt, Arthur, G., Lee, J.-Y., Kachroo, A., Kachroo, P., 2016. Plasmodesmata localizing proteins regulate transport and signaling during systemic acquired immunity in plants. Cell Host Microbe 19, 541–549.

Maffei, M.E., Mithofer, A., Arimura, G.I., Uchtenhagen, H., Bossi, S., Bertea, C.M., Cucuzza, L.S., Novero, M., Volpe, V., Quadro, S., Boland, W., 2006. Effects of feeding *spodoptera littoralis* on lima bean leaves. III. Membrane depolarization and involvement of hydrogen peroxide. Plant Physiol. 140, 1022–1035.

Mersmann, S., Bourdais, G., Rietz, S., Robatzek, S., 2010. Ethylene signaling regulates accumulation of the FLS2 receptor and is required for the oxidative burst contributing to plant immunity. Plant Physiol. 154, 391–400.

Mithöfer, A., Mazars, C., Maffei, M.E, 2009. Probing spatio-temporal intracellular calcium variations in plants. Methods Mol. Biol. 479, 79–92.

Osmont, K.S., Sibout, R., Hardtke, C.S., 2007. Hidden branches: developments in root system architecture. Annu. Rev. Plant Biol. 58, 93–113.

Parmagnani, A.S., Kanchiswamy, C.N., Paponov, I.A., Bossi, S., Malnoy, M., Maffei, M.E., 2023. Bacterial volatiles (mVOC) emitted by the phytopathogen Erwinia amylovora promote arabidopsis thaliana growth and oxidative stress. Antioxidants 12, 600.

Rahman, A., Takahashi, M., Shibasaki, K., Wu, S., Inaba, T., Tsurumi, S., Baskin, T.I., 2010. Gravitropism of Arabidopsis thaliana roots requires the polarization of PIN2 toward the root tip in meristematic cortical cells. Plant Cell 22, 1762–1776.

Roychoudhry, S., Sageman-Furnas, K., Wolverton, C., Grones, P., Tan, S., Molnár, G., De Angelis, M., Goodman, H.L., Capstaff, N., Lloyd, J.P.B., Mullen, J., Hangarter, R., Friml, J., Kepinski, S., 2023. Antigravitropic PIN polarization maintains non-vertical growth in lateral roots. Nat. Plants 9, 1500–1513.

Ryu, C.-M., Farag, M.A., Hu, C.-H., Reddy, M.S., Kloepper, J.W., Paré, P.W., 2004. Bacterial volatiles induce systemic resistance in Arabidopsis. Plant Physiol. 134, 1017–1026.

Ryu, C.-M., Farag, M.A., Hu, C.-H., Reddy, M.S., Wei, H.-X., Paré, P.W., Kloepper, J.W, 2003. Bacterial volatiles promote growth in Arabidopsis. Proc. Natl. Acad. Sci. USA 100, 4927–4932.

Saatian, B., Kohalmi, S.E., Cui, Y., 2023. Localization of Arabidopsis glucan synthase-like 5, 8, and 12 to plasmodesmata and the GSL8-dependent role of PDLP5 in regulating plasmodesmal permeability. Plant Signal. Behav. 18, 2164670.

Schulz-Bohm, K., Martín-Sánchez, L., Garbeva, P., 2017. Microbial volatiles: small molecules with an important role in infra- and inter-Kingdom interactions. Front. Microbiol. 8, 10.

Semeradova, H., Montesinos, J.C., Benkova, E., 2020. All roads lead to Auxin: post-translational regulation of Auxin transport by multiple hormonal pathways. Plant Commun. 1, 100048.

Sharifi, R., Ryu, C.M., 2018. Sniffing bacterial volatile compounds for healthier plants. Curr. Opin. Plant Biol. 44, 88–97.

Tee, E.E., Faulkner, C., 2024. Plasmodesmata and intercellular molecular traffic control. New Phytol. 243, 32–47.

Ulmasov, T., Murfett, J., Hagen, G., Guilfoyle, T.J., 1997. Aux/IAA proteins repress expression of reporter genes containing natural and highly active synthetic auxin response elements. Plant Cell 9, 1963–1971.

Vieten, A., Vanneste, S., Wisniewska, J., Benková, E., Benjamins, R., Beeckman, T., Luschnig, C., Friml, J., 2005. Functional redundancy of PIN proteins is accompanied by auxin-dependent cross-regulation of PIN expression. Development 132, 4521–4531.

Waidmann, S., Ruiz Rosquete, M., Schöller, M., Sarkel, E., Lindner, H., Larue, T., Petřík, I., Dünser, K., Martopawiro, S., Sasidharan, R., Novak, O., Wabnik, K., Dinneny, J.R., Kleine-Vehn, J., 2019. Cytokinin functions as an asymmetric and anti-gravitropic signal in lateral roots. Nat. Commun. 10, 3540.

Wang, X., Sager, R., Cui, W., Zhang, C., Lu, H., Lee, J.Y., 2013. Salicylic acid regulates plasmodesmata closure during innate immune responses in Arabidopsis. Plant Cell 25, 2315–2329.
Wankhade, A., Wilkinson, E., Britt, D.W., Kaundal, A., 2025. A review of plant–Microbe interactions in the rhizosphere and the role of root exudates in microbiome engineering. Appl. Sci. 15, 7127.
Weisskopf, L., Schulz, S., Garbeva, P., 2021. Microbial volatile organic compounds in intra-kingdom and inter-kingdom interactions. Nat. Rev. Microbiol. 19, 391–404.
Wendehenne, D., Durner, J., Klessig, D.F., 2004. Nitric oxide: a new player in plant signalling and defence responses. Curr. Opin. Plant Biol. 7, 449–455.
Zanini, A.A., Burch-Smith, T.M., 2024. New insights into plasmodesmata: complex 'protoplasmic connecting threads. J. Exp. Bot. 75, 5557–5567.
Zhao, W., Chen, X., Wang, J., Cheng, Z., Ma, X., Zheng, Q., Xu, Z., Zhang, F., 2025. Emerging mechanisms of plant responses to abiotic stress. Plants 14, 3445.
Zipfel, C., Robatzek, S., Navarro, L., Oakeley, E.J., Jones, J.D.G., Felix, G., Boller, T., 2004. Bacterial disease resistance in Arabidopsis through flagellin perception. Nature 428, 764–767.